Mechanical force sensing drives extrusion of Enterovirus A71-infected cells from colonic epithelial organoids

Jasmine Moshiri
Stanford University
Ailsa Craven
Stanford University
Sara Mixon
Stanford University
Manuel Amieva
Stanford University https://orcid.org/0000-0002-5601-4490
Karla Kirkegaard (karlak@stanford.edu)
Stanford University

Article

Keywords:

Posted Date: August 15th, 2022

DOI: https://doi.org/10.21203/rs.3.rs-1915730/v1

Mechanical force sensing drives extrusion of Enterovirus A71-infected cells from colonic epithelial organoids

Jasmine Moshiri[1], Ailsa Craven[2], Sara Mixon[2], Manuel Amieva[1,3], Karla Kirkegaard[1,2]

[1]Department of Microbiology and Immunology, Stanford University, Stanford, CA 94304, USA.

[2]Department of Genetics, Stanford University, Stanford, CA 94304, USA.

[3]Department of Pediatrics, Stanford University, Stanford, CA 94304, USA.

Abstract

Enterovirus A71 (EV-A71) causes severe disease upon systemic infection, sometimes leading to life-threatening neurological dysfunction. In most cases, infection is limited to the gastrointestinal tract, where virus is amplified for transmission. We used three-dimensional epithelial organoids generated from crypt stem cells of healthy patient colon tissue (colonoids) to investigate viral spread. Surprisingly, many infected cells were extruded from the apical surface of colonoids, leading to their removal from the epithelium. EV-A71 infected extruding cells were not frequently apoptotic and could propagate infection to uninfected monolayers and colonoids. Cell extrusion in healthy gastrointestinal epithelium is mediated either by apoptosis or cell-crowding forces sensed via the mechanosensitive ion channel Piezo-1. Treatment of infected colonoids with mechanosensitive ion-channel inhibitor GsMTx4 significantly reduced the infected cell extrusion. Instead, increased abundance of cell-free virus in media was observed. These results suggest a novel mechanism for extrusion of live, virus-infected cells through mechanical compression forces. In the gastrointestinal tract, apically extruded cells are released into the gut lumen and excreted in feces; therefore, extruded infected cells likely contribute to virus spread.

Introduction

The question of how progeny viruses leave an infected cell or tissue is vital to our understanding of viral spread throughout an infected host and between hosts. For decades picornaviruses, as nonenveloped or “naked” viruses, were thought to transmit strictly lytically, through dramatic rupture of the infected cell. Lytic release of picornaviruses from standard tissue culture cell lines results in widespread dispersal of virions to initiate subsequent rounds of infection. However, nonlytic spread has been demonstrated for several picornaviruses. In poliovirus-infected cells, the intracellular formation of double-membraned vesicles allows the extracellular release of infectious virus within vesicles that bear autophagy marker LC3 in a process akin to secretory autophagy [1–3]. Hepatitis A virus was found to egress from infected cells cloaked in membranes from the host multivesicular body pathway [4]. In both cases, picornaviruses appropriated intracellular membranes to facilitate their release from intact cells, cloaked within extracellular vesicles. One consequence of this transmission strategy is that, instead of the dispersive spread of single viral particles, viruses are transmitted *en bloc* within membranous packets [5,6].

Epithelial organoid models are exciting tools to examine tissue-wide dynamics. Organoids derived from induced pluripotent stem cells, fetal tissue stem cells, and adult tissue stem cells are all attractive candidates for examining tissue-specific responses to pathogenic insults [7,8]. Adult stem cell-derived 3D spherical organoids can be differentiated to recapitulate the diversity of cell types present in native tissues [9]. Organoids typically grow with their apical surfaces facing interior lumenal compartments. 2D polarized monolayers or organoids that were mechanically sheared to allow apical access of EV-A71 have been used to model EV-A71 infection of the gastrointestinal epithelium [10–12]. Recently, methods to invert organoid topology have been developed to present the apical surface of gastrointestinal epithelia to enteric pathogens directly while preserving epithelial integrity [13,14]. These apical-out organoids are used here to monitor the infection of epithelial cells by EV-A71 and subsequent mechanisms of viral spread.

EV-A71 is a member of the Enterovirus genus in the *Picornaviridae* family of single-stranded, positive-sense RNA viruses. EV-A71 is a major causative agent of Hand, Foot and Mouth Disease, and systemic infection may lead to severe neurological dysfunction, especially in infants and young children.

However, the seroprevalence of EV-A71 in endemic areas indicates that the majority of infections are asymptomatic [15,16]. Importantly, even those asymptomatically infected can shed virus for several weeks in feces [17].

Using differentiated apical-out colonoids, we evaluated the morphological characteristics of EV-A71-infected cells. Little cell-to-cell spread within the organoids was observed. Instead, infected cells were specifically expelled from otherwise intact colonoids by whole-cell extrusion. The extruded infected cells were predominantly not apoptotic, and inhibition of apoptotic caspases did not prevent extrusion. However, inhibiting the activity of mechanosensitive ion channels caused infected cells to be retained within the colonoids. Thus, mechanosensation plays a key role in the response of intact epithelial tissues to viral threats. Extruded cells were found to carry live virus and the intact extruded cells were competent to initiate new infections. This mechanism may facilitate viral release into the intestinal lumen, spread within the host, and fecal transmission during natural infection.

Results

Apical-out colon organoids are permissive to EV-A71 infection.

We were interested in using apical-out gastrointestinal epithelial organoids as a model of EV-A71 infection in which epithelial barrier integrity is maintained. We chose to use organoids derived from colonic tissue (colonoids) due to the proximity of the colon to viral exit from an infected host to better understand EV-A71 transmission. Colonoids derived from adult human crypt tissue were grown on basement membrane scaffolds in the presence of stem factors, including WNT and R-spondin, generating spheroids of stem cells with their basolateral surface facing outwards and their lumenal, apical surfaces facing inwards. At five days before infection, colonoids were removed from the basement membrane scaffold and kept in suspension culture in the absence of matrix to induce the reversal of organoid topology so that the apical surfaces were on the organoid exterior (apical-out) [13]. At the same time, medium to induce cell differentiation was applied. To determine whether the apical-out colonoids mimicked the apical surface of the human colon, we monitored the organization of the actin cytoskeleton and EV-A71 receptor SCARB2 (Fig. 1A). The apical surface of well-differentiated and polarized colonoids contains brush border microvilli easily identifiable with F-actin staining as a thick, actin-rich layer. SCARB2 is an integral lysosomal membrane protein that cycles to the apical surface of polarized monolayers [18,19] and was abundantly expressed in these apical-out colonoids (Fig. 1A).

Viral growth curves beginning immediately after infection showed that EV-A71 could productively infect differentiated apical-out colonoids from two different human donors, with virus accumulation in the entire culture continuing up to 48 hours after infection (Fig. 1B). After 48 hours, infected colonoids were fixed and stained for the presence of double-stranded viral RNA (vRNA), a collapsed RNA replication intermediate, to identify infected and uninfected cells by confocal microscopy. Punctate juxtanuclear and cytoplasmic staining patterns indicative of viral RNA replication complexes were readily observed (Fig. 1C). Curiously, the majority of infected cells were solitary amidst their uninfected neighbors.

EV-A71 infected cells are extruded from colonoids

The lack of observable viral spread, even as viral yield was increasing, could be rationalized following careful inspection of the apical surfaces of the infected colonoids. We were surprised by the

frequent observation of virus-infected cells that appeared to be extruding from intact colonoids (Fig. 2A-C). In the gastrointestinal epithelium, whole cell extrusion maintains homeostatic cell numbers by facilitating removal of existing cells to match the rate of stem cell expansion in the crypts. In fact, so many cells are extruded that the average lifespan of a gastrointestinal epithelial cell is just 2-5 days [20–22]. To determine whether the frequencies at which EV-A71 infected cell extrusion exceeded those of uninfected cells, we quantified how frequently both infected and uninfected cells underwent extrusion from the same EV-A71-infected colonoids (Fig. 2D-2F). Infected colonoids were fixed, stained, and examined by confocal microscopy. Individual cells were categorized as 1) infected or uninfected and 2) extruding or non-extruding. A cell was defined as extruding from an organoid if its nucleus had crossed the apical border of the organoid, visualized by staining with phalloidin to monitor the localization of the cortical actin. At the 48-hour timepoint examined, 40% of the infected cells were extruding, compared to only 1% of the uninfected cells (Fig. 2D, 2F). Similarly, although infected cells constituted only 0.4% of the cells within the organoids, they constituted 25% of the extruding cells (Fig. 2E, 2F). These data demonstrate that infected cells are extruded from colonoids at frequencies significantly higher than expected by random chance. Furthermore, previous observations of villous blunting in the intestines of EV-A71-infected mice are consistent with such increased expulsion of infected cells from the gastrointestinal epithelium [23,24].

To investigate whether the phenomenon of infected cell extrusion was specific to EV-A71, we examined cells infected with poliovirus, a member of the related Enterovirus C species. In organoids derived from ileal tissue of the small intestine as well as colonic tissue, extruding poliovirus-infected cells were readily observed (Fig. S1). We suggest that multiple enteroviruses instigate the ejection of infected cells from gastrointestinal organoids by whole-cell extrusion.

We observed infected cells in several distinct states reminiscent of the stages of canonical whole-cell extrusion (Fig. 2G-H). Cell extrusion is a highly coordinated process that allows the removal of undesirable cells while maintaining the integrity of the epithelial barrier [25–27]. During canonical extrusion, cells fated for extrusion and their neighboring cells rearrange their cytoskeletons to surround the base of the extruding cells; these actin-myosin rings contract apically to squeeze out the cells being extruded by what has been termed a 'purse-string' mechanism (Fig. 2H) [28]. At the same time, tight junctions re-form

between the new neighbor cells below the extruding cells to maintain epithelial integrity [29,30]. Cell displacement and formation of new neighbors occur over a period of approximately 40 minutes. Extruded cells cling to the epithelium for an additional 40 minutes before detaching from their neighbors and floating away [28,31]. We observed infected cells in states consistent with both early and late stages of extrusion, as shown in Fig. 2G. At left, an infected cell can be seen embedded within an organoid, surrounded by an actin layer condensing beneath the infected cell. The middle image shows an extruded cell still in contact with a re-formed, intact apical surface. The fully detached infected cell at right was observed floating in suspension alongside infected organoids.

To identify the permissive cell type in the colonoids, we performed immunostaining with antibodies targeting Villin1 and Muc2, expressed by absorptive colonocytes and goblet cells, respectively (Fig. 2I-L). Both cell types have been previously implicated in EV-A71 infection in the gastrointestinal epithelium [11,12]. Our observations suggest that absorptive colonocytes, rather than goblet cells, were the primarily infected cell type in this model. This finding does not preclude infection of goblet cells in epithelia in which goblet cells are more plentiful.

To characterize the timing of infected cell extrusion, we quantified the number of infected cells within colonoids over a time course during the first round of infection (Fig. S2). We noted that the number of infected cells increased significantly from five to seven hours after infection, but substantially reduced afterwards, even though the amount of infectious virus in the entire culture continued to rise (Fig. 1B). That infected cells are predominately shed between seven to nine hours after infection is consistent with the lack of observed cell-to-cell transmission within the colonoids. The small increase in viral titer within the culture after nine hours (Fig. 1B) could therefore indicate modest spread within the organoid, re-infection of the organoid by the extruded cells or continued amplification within the extruded cells.

EV-A71-infected cells that extrude from organoids are predominantly not apoptotic

Extrusion of apoptotic cells from intact epithelia was originally described as a means to remove dying cells without compromising the epithelial barrier [28]. Given that EV-A71 infection can trigger apoptosis in several cell types [32–35], we tested whether apoptotic signaling was the trigger for extrusion of

infected cells in colonoids. We utilized a fluorogenic substrate (CellEvent, ThermoFisher) to visualize cells that expressed active caspases 3 and 7. Infected organoids were incubated with substrate, fixed, stained for double-stranded RNA, and examined by confocal microscopy (Fig. 3A-E). Approximately half of the uninfected extruded cells were caspase 3/7 positive, consistent with the normal functioning of cell extrusion in intestinal epithelia [36]. However, a significantly lower fraction of infected, extruding cells were caspase 3/7 positive (Fig. 3F-G). Furthermore, the nuclei in infected extruding cells were usually intact and did not display the condensed and fragmented nuclei characteristic of apoptotic cells. These data argue that apoptotic stress is not the trigger of infected cell extrusion.

Mechanosensing ion channel activity mediates EV-A71 infected cell extrusion

In addition to apoptotic or pyroptotic cell death, cell extrusion from the gastrointestinal epithelium can be triggered by mechanical forces on cells due to overcrowding [37,38]. Although it plays no role in extrusion of apoptotic cells, the mechanosensitive ion channel Piezo-1 senses and responds to cell crowding stress, triggering cell extrusion [36]. We hypothesized that alteration of the biomechanical properties of infected cells may be sensed by Piezo-1, leading to force-dependent extrusion of infected cells. To test this hypothesis, we treated infected colonoids with GsMTx4, a spider venom peptide that inhibits the activity of mechanosensitive ion channels including Piezo-1 [39,40]. We also evaluated the effect of Z-VAD-FMK, a pan-caspase inhibitor known to reduce apoptotic cell extrusion [31,41]. Finally, given that actin-myosin rearrangement is critical for cell extrusion regardless of initial trigger, we tested the effect of myosin II inhibitor para-nitro-Blebbistatin [42] as a positive control for inhibition of all cell extrusion mechanisms [43,44] (Fig. 4E).

Following two hours of infection with EV-A71, colonoids were treated with compounds above for the remainder of a single cycle of infection (Fig. 4A-D). The proportion of infected cells extruding from colonoids was quantified under each condition (Fig. 4F). As expected, the percentage of infected cells extruding from organoids was significantly reduced in the presence of blebbistatin and unaffected by Z-VAD-FMK, which inhibits only apoptotic extrusion. However, we observed a significant and striking reduction in the percentage of infected cells undergoing extrusion in the presence of mechanosensitive ion channel inhibitor GsMTx4 (Fig. 4F). To exclude the possibility that this was due to inhibition of viral growth, we evaluated the effect of all compounds on viral yield, none of which were changed (Fig. 4G).

These results argue that it is the force-sensing activity of mechanosensitive ion channels targeted by GsMTx4 that is crucial for the elimination of live, EV-A71-infected cells.

The fate of extruded infected cells

To determine whether the extruded, infected cells could provide a source of viral spread within the gastrointestinal tract, extruded cells were isolated by differential sedimentation and the amount of virus within them was determined. Briefly, entire suspensions of organoid culture (*Whole Well*) were collected. Then, organoid-free *(Cells + Media)* preparations that contained extruded *Cells* and cell-free media were collected, with visual confirmation of organoid removal by confocal microscopy. To confirm that subsequent washing steps would efficiently remove cell-free virus, 10^6 plaque-forming units of exogenous virus were spiked into to a set of *(Cells + Media)* samples. Extruded *Cells* were then pelleted by centrifugation and washed thoroughly remove any residual cell-free virus. All collected samples were subjected to repetitive freeze/thaw to release intracellular virus in cell-containing fractions and viral titers were determined by plaque assay. The spiked-in virus greatly increased the viral titer in *Cells + Media* samples (Fig. 5B). However, the viral titer in the *Cells* was unchanged by the spike-in of exogenous virus, demonstrating that the repeated washes successfully eliminated potential contaminating free virus. Additionally, as shown in Figure 5C, there was significantly more infectious virus in the extruded *Cell* fractions than in cell-free *Media.*

To determine how long the extruded cells remained alive after extrusion, we monitored the apoptotic state of *Cells* after 48 hours of continued incubation. At that time point, the majority of both infected and uninfected extruded cells were caspase 3/7-positive (Fig. S3), suggesting that cells extruded as a result of viral infection eventually undergo *anoikis* (detachment-induced apoptotic cell death). To test whether residence within these dying, extruded cells damaged the resident virions, *Cell* and *Media* preparations shown in Figure 5C were incubated at 37 °C. All samples were subjected to repetitive freeze thaw cycles to lyse cells prior to plaque assay. Over a 27-hour time course, virus residing within *Cells* retained stability slightly longer than free virus in *Media* (Fig. 5D). Therefore, infected cells expelled from colonic epithelia contain stable, infectious virus.

To elucidate whether extruded cells are themselves infectious, *Cells* fractions were prepared from infected colonoids and used as inocula for secondary infections (Fig. 5E, F). Viral growth in both secondarily infected RD cell monolayers and previously uninfected colonoids was examined by comparing titers immediately after infection and after 16 hours of infection. As a control for effective isolation of *Cells* from any remaining free virus, supernatants from the last of three washes were also used as inocula. In cultures infected with cells extruded from previously infected organoids, abundant virus was present immediately after infection (Fig. 5E, F) and significant increases were observed upon incubation. Importantly, after 16 hours the quantity of virus in cultures infected with extruded cells was significantly higher than that in cultures infected with wash supernatant, indicating that the presence of extruded cells, rather than residual cell-free virus, was responsible for the high viral loads. Confocal microscopy confirmed the presence of infected cells within secondarily infected RD monolayers and colonoids (Fig. 5G, H). Therefore, extruded, virus-containing cells are infectious to both RD monolayers and apical-out, differentiated colonoids.

The fate of infected cells retained within colonoids

To determine the fate of the viruses and cells retained in the colonoid epithelial layer when extrusion was inhibited, colonoids were infected with EV-A71 and *Whole Well*, *Organoid*, *Cells* and *Media* fractions (Fig. 5A) were collected by differential sedimentation. Samples were subjected to cycles of freezing and thawing to release intracellular virus prior to plaque assay. As expected, inhibition of force sensing by treatment with GsMTx4 did not affect overall viral growth, as evidenced by the *Whole Well* fraction, although significantly less virus was found in the extruded *Cells* fraction. The amount of infectious virus within intact organoids was unaffected by GsMTx4 treatment, even though the release of infected cells was blocked. Instead, significantly more virus was observed in the *Media* fraction when extrusion was blocked (Fig. 5I). We surmise that the extrusion of cells from the epithelial layer prevents the outcome that would otherwise occur: the release of cell-free virus.

Discussion

Infected cells experience a variety of metabolic, oxidative and misfolding stresses that trigger innate cellular responses such as apoptosis, autophagy and the synthesis of inflammatory mediators. Successful viruses inhibit or subvert many of these responses to enhance viral replication. Here, we report that enterovirus A71 (EV-A71) also affects mechanosensory signaling pathways. In the polarized cells of colon organoids, EV-A71-infected cells are preferentially extruded into the apical extracellular milieu that corresponds to the colonic lumen. This process could be both advantageous to the host, by eliminating infected cells from the intestinal epithelium and for the viral population, whose collective extrusion likely facilitates inter-host transmission.

To study EV-A71 infections of the human gastrointestinal epithelium, we utilized an adult stem cell-derived epithelial organoid model of infection. Given that the natural route of infection for EV-A71 is via the apical surface of the intestinal epithelium, we chose to investigate viral spread in differentiated, apical-out organoids from human colon. Most EV-A71-infected cells were, to our surprise, actively extruded from the apical surface of the infected colonoids. This was also observed in colonoids infected with poliovirus, another member of the Enterovirus genus. This extrusion of infected cells occurred predominantly within the first seven to nine hours of infection, occurring within the first infectious cycle. Little cell-to-cell spread was observed. Instead, cells that neighbored the infected cells rearranged their actin-myosin contractile fibers in stages that resemble previously-described whole cell extrusion events (Fig. 2G) [28].

In the canonical whole-cell extrusion that is required for the homeostasis of polarized epithelia, an actin-myosin ring forms around the base of the extruding cell, then contracts to remove the cell while maintaining neighbor cell contacts within the intact epithelium. This process is often accompanied by apoptotic signaling from the cell that is to be extruded. EV-A71 has been shown to induce apoptosis in several tissue culture cell lines, including colorectal adenocarcinoma epithelial cells [33]. However, the extrusion of EV-A71-infected cells from intact colonoids occurred largely without apoptotic signaling and was independent of the activity of apoptotic caspases. Clearly, the cell type and differentiation state of

EV-A71-infected cells affects the host response to infection, demonstrating the usefulness of models that recapitulate the natural infection of interest as faithfully as possible [10,45,46].

A second signaling pathway that leads to whole-cell extrusion in intestinal epithelia is the crowding stress sensed by force-dependent ion channels. In this work, we showed that the extrusion of EV-A71-infected enterocytes from polarized human colonoids is hindered by the small peptide GsMTx4, an inhibitor of mechanosensitive ion channels [40,47]. These data implicate force sensing as the trigger for extrusion of infected cells. In cultured polarized monolayers and intestinal epithelia, force-sensitive ion channel Piezo1 is known to act as a sensor for cell density homeostasis [36,48]. When epithelia are overcrowded, Piezo1 induces extrusion of live, non-apoptotic cells until homeostatic cell numbers are re-established [36]. Piezo proteins are plasma membrane-embedded homotrimers, with propeller-like arms and a central Ca^{+2}-permeable pore [49]. Upon deformation of the plasma membrane by mechanical force, the arms are thought to reposition, inducing a conformational change in which the pore opens [49]. We postulate that Piezo1 is a likely candidate for the force-driven extrusion of infected cells reported here.

Enteroviruses are known to cause global reorganization of host cell components including all cytoskeletal elements[50–52]. Indeed, drastic cytoskeletal rearrangements are major contributors to the oft-used description of the ‘cytopathic effect’ caused by many viruses [53,54]. Reduction in both membrane tension and cytoskeletal tethering have been implicated in Piezo1 activation [55]. In this study, we observed that the infected cells extruding from human colonoids were rounded and had lost the actin microvilli on their apical surfaces. It is possible that, due to this disruption, it is the difference between the biomechanical properties of EV-A71-infected cells and their uninfected neighbors that leads to the extrusion of the infected cells.

The removal of infected cells by mechanical cell competition might benefit the host by limiting local viral spread in infected tissue. In addition, when extrusion was blocked, an increase in extracellular virus was observed, suggesting that infected cells forced to remain within organoids release virus into the medium through lysis or unconventional secretion. If infected cells are on the verge of lysis, their

extrusion could benefit the host by maintaining the epithelial barrier, by reducing inflammation, or both (Fig. 6).

Extruded cells could also serve as a means for viral spread from one region of gastrointestinal tissue to a more distal region in the same host, or to another host (Fig. 6). We found that EV-A71-infected cells themselves are infectious to both cell monolayers and previously uninfected organoids. Transiting through the colon within an extruded cell might protect virions from luminal contents such as mucosal antibodies (Fig. 6). Such *en bloc* viral delivery can have several consequences, due to the transmission of concentrated virus and the maintenance of the complexity of the intracellular viral quasispecies population [5,6,56,57].

Our findings add to a growing body of evidence that intracellular pathogens can be removed from epithelial layers through the controlled ejection of infected cells via a variety of mechanisms. Rotavirus, Reovirus, Respiratory Syncytial Virus, and *Salmonella* all trigger pyroptotic or apoptotic cell death in single infected cells that are subsequently extruded [38,58–61]. In contrast, *Listeria* and Measles virus both induce massed shedding, with scores of live infected cells forming large mounds that aggregate atop polarized epithelia [44,62]. The unique phenomenon of force-dependent single-cell extrusion of infected cells described here may accompany infection with additional intracellular pathogens that remain to be identified.

In summary, these findings identify the phenomenon of live extrusion of virus-infected cells initiated by mechanosensitive ion-channel activity. Mechanosensitive extrusion may serve a crucial innate immune function by initiating the expulsion of infected cells from epithelial tissue. Furthermore, given that extruded cells can initiate further viral infection, shedding of virus-infected cells may serve as a previously unappreciated means of fecal-oral transmission.

Acknowledgements

We thank Julia Co, Mar Margalef-Català and Kuo-Feng Weng for sharing expertise and reagents, Calvin Kuo for the generous provision of organoid cell lines, and Peter Sarnow and Jan Carette for critical reading of the manuscript. This work was supported by the Chan-Zuckerberg BioHub (KK), BioX of Stanford University (AC), Novo Nordisk Foundation grant NNF19OC0056411 (MA), and National Institutes of Health grants R01AI13491204 (KK), 5U19AI116484-06 (MA), T32GM007276 (JM) and T32AI1007328 (JM).

Materials and Methods

Epithelial organoids cultivation and growth

Organoids were generated following the principles described by Toshiro Sato, Hans Clevers, and colleagues [9]. Gastrointestinal epithelial organoids derived from healthy adult patient tissue biopsies were generated by the lab of Calvin Kuo at Stanford University [14]. For maintenance, organoids were seeded within Cultrex Reduced Growth Factor Basement Membrane Matrix, Type II (BME, equivalent to Matrigel) in droplets within a 24-well tissue culture treated plate (40 µL/well). BME was polymerized by incubation for 10 min at 37°C, then growth media was overlaid atop BME. Growth media consists of: Advanced Dulbecco's modified Eagle medium/F12, 1 mM HEPES, 1x Glutamax, 1x B27 (without vitamin A), 1 mM N-Acetyl-cysteine (for intestinal and colonic samples only), 10 nM Gastrin, 50 ng/mL EGF, 10 mM Nicotinamide, 500 nM A83-01, 10 µM SB202190, 100 ng/mL FGF10 (for gastric samples only) and 50% L-WRN-conditioned media (contains Wnt3a, R-spondin 3, and Noggin, see details below). L-WRN conditioned media was prepared from L-WRN cells as previously described [63]. L-WRN conditioned media was aliquoted and frozen at -80°C for long-term storage with no negative effects on organoid growth observed. Growth media was replaced every 1-4 days as needed.

To passage, organoids were dissociated to single cells in TypLE Express for 10-15 min at 37°C, manually disrupted by pipetting, then trypsin was inactivated with FBS. On ice, cells were filtered through a 70 µm-pore nylon mesh cell strainer to remove large clumps of cells or undissociated organoids. Cells were counted on a Countess II Cell Counter (ThermoFisher) and reseeded in BME at a concentration of 5 $\times 10^3$ – 1.5 $\times 10^4$ cells per well. For 2-3 days after initial passage, 10 µM Y27623 and 250 nM CHIR99021 were included in growth media to prevent detachment mediated cell death. Organoids were passaged every 4 – 10 days as needed. All organoids used were tested with Myco-Sniff™ (MP Biomedicals) to ensure no mycoplasma contamination was present.

Epithelial organoids differentiation and polarity reversal

After 4 – 7 days of growth, organoids were removed from Matrigel and induced to revert their polarity in order to expose the apical surface using a previously published procedure [13]. Organoids were incubated in 5 mM EDTA in phosphate buffered saline (PBS) at 4°C for 40 min, washed with DMEM, and

resuspended in differentiation media: Advanced Dulbecco's modified Eagle medium/F12, 1 mM HEPES, 1x Glutamax, 1x B27, 1 mM N-Acetyl-cysteine (for intestinal and colonic samples only), 10 nM Gastrin, 50 ng/mL EGF, 10 ng/mL Noggin, 500 nM A83-01, 5 µM γ-Secretase Inhibitor IX (also known as DAPT, colonic samples only), 100 ng/mL FGF10 (for gastric samples only), and 10 µM Y27623. Organoids in suspension culture were plated in ultra-low attachment plates or flasks (Corning Costar) and incubated at 37°C for 5 days to complete differentiation and polarity reversal prior to experimental use.

Rhabdomyosarcoma cells and virus propagation

Rhabdomyosarcoma (RD) cells were cultured in DMEM (Hyclone; 4500 mg/L glucose, 4 mM L-Glutamine, 1 mM sodium pyruvate) supplemented with 10% fetal bovine serum (Omega Life Sciences), 1x non-essential amino acids (MEM NEAA, Gibco), and 1x penicillin/streptomycin (Gibco). RD cells were grown at 37°C with 5% CO_2. EV-A71 strain 4643 was amplified from an infectious clone produced by the lab of Jen-Ren Wang using RD cells as previously reported [64]. The full cDNA sequence of the virus strain used can be found under GenBank Accession number JN544418. Virus stocks from the 2nd viral passage in RD cells were generated and utilized for infections. Viral titer was determined by plaque assay on RD cells, using a 0.3% (w/v) agarose overlay; plaques were fixed after 3 days with 2% formaldehyde and enumerated by staining with crystal violet.

EV-A71 infections of organoids

Differentiated, apical-out organoids (five days post-differentiation and polarity reversal) were infected with EV-A71 strain 4643. As RD cells are highly susceptible to EV-A71 infection, multiplicity of infection as defined by RD cells corresponds to a much sparser infection in organoids. Organoids were therefore exposed to a high multiplicity of infection (MOI, 620 PFU/cell) to establish an infection in which five or fewer cells were infected per organoid. Apical-out organoids were prepared from colonic, gastric and duodenal tissues and infected with EV-A71. Between these three tissues, colonoids were the most robustly infected (Fig. S4, Fig. 1B).

To separate organoids in suspension from debris prior to infection, organoids were collected in a 15-mL conical tube and allowed to pellet by gravity on the benchtop (1 × *g*) for 5 – 10 min. Supernatant was discarded, and pelleted organoids were washed once in DMEM. An aliquot of this organoid

suspension was removed, dissociated with TrypLE Express, and counted on Countess II Cell Counter (ThermoFisher) to enumerate cells in organoid suspension for MOI calculations. For experiments in which triplicate infections were performed, organoid suspension was divided into three conical tubes. Organoids were pelleted at 300 × *g* for 3 min and resuspended in appropriate volume of virus stock (3.7E8 PFU/mL), transferred to an ultra-low attachment plate, and incubated at 37°C with 5% CO_2 for 2 h. After incubation, organoids were washed three times in DMEM with centrifugations at 300 × *g* for 3 min. After the 3rd wash, organoids were resuspended in warm differentiation media and plated into ultra-low attachment tissue culture plates. Pharmacological treatments were then added if applicable. Infected organoids were incubated at 37°C with 5% CO_2 until the experimental endpoint. In experiments during which overall viral titer was quantified, the entire organoid suspension was collected, and the sample was subjected to three repeated freeze/thaw cycles to lyse cells prior to plaque assay.

Confocal microscopy

Organoids were fixed in 2% paraformaldehyde in 100 mM sodium phosphate buffer (pH 7.4) for at least 30 minutes and washed with PBS. Organoids were stained by incubating with antibodies and/or stains in blocking/permeabilization buffer (PBS with 3% bovine serum albumin, 1% saponin, and 0.02% sodium azide) overnight with gentle agitation. Stained organoids were washed 3x in PBS, mounted onto glass slides using Vectashield mounting medium (Vector Laboratories, H-1000), and glass coverslips were affixed using vacuum grease. Organoids were imaged on a LSM 700 confocal microscope (Carl Zeiss) with Zen 2009 software (Carl Zeiss) at 40x or 63x magnification with oil immersion objectives. 3D renderings of organoids were generated using Volocity 3D Image Analysis Software (Perkin Elmer).

Organoids were stained with DAPI (4',6-Diamidino-2-Phenylindole, Dihydrochloride, Life Technologies, D1306) and Alexa Fluor 660 phalloidin (Invitrogen, A22285) to visualize nuclei and actin. Primary antibody dilutions were performed at the following dilutions: anti-dsRNA (1:500), anti-LIMP2/SCARB2 (1:100), anti-Muc2 (1:200) and anti-Vil1 (1:100). Secondary antibody (Invitrogen Cross-Absorbed) dilutions were performed at 1:500 dilution. Secondary antibodies included in the same organoid staining procedure were raised in the same host species (Goat). For visualization of caspase 3/7 activity, CellEvent^{TM} Caspase 3/7 Green Detection Reagent (Invitrogen, C10723) was added to live organoids at 10 µM after 24 h infection, then organoids were fixed at 48 hpi and stained as described

above. Single cells that had been fully extruded from organoids were stained and imaged in the same manner as intact organoids as described above, however for these experiments a 20x magnification dry objective was used.

Quantitation of microscopy data

Organoid images were viewed using Volocity 3D Image Analysis Software (Perkin Elmer) to gain 3D visualization of each organoid. Cells within organoids that were considered extruding, apoptotic, and/or infected were manually counted. An extruding cell was defined by a cell attached to an organoid with a nucleus that has transversed the organoid microvillus brush border. In experiments requiring counting of all cells, the total number of cells in each organoid was enumerated by imaging DAPI at 6 µm z-stack intervals to capture the nuclei of each organoid cell in a single z-plane. Volocity was used to quantify individual nuclei from these individual z-plane images using the 2D Nuclei quantitation feature. In relevant experiments, quantification of remaining non-extruding or uninfected cells were calculated by subtracting the number of manually counted cells in each group from the total number of cells in each organoid.

In experiments where fully extruded cells were examined, individual cells were identified from 3D renderings of images with z-stacks at 1.8 µm intervals. Volocity 3D Image Analysis Software (Perkin Elmer) was used to identify individual cells: nuclei were first identified using the Find Objects quantitation feature, object area was increased to surround each nucleus using the Dilate Objects quantitation feature twice iteratively, and signal intensity in each channel was captured using the Measure Objects feature. Objects with a Sum intensity in vRNA channel > 2500 were considered infected.

Inhibitor treatments

Pharmacological compounds and peptides were tested for their ability to reduce infected cell extrusion. For all experiments, organoids were exposed to compounds after initial viral inoculation and washing steps. Z-VAD-FMK (pan-caspase inhibitor, R&D Systems, 21631) and para-nitro-Blebbistatin (Myosin II inhibitor, Cayman Chemical, 24171) were solubilized in anhydrous DMSO and added to infected organoids at final concentrations of 100 µM and 50 µM, respectively. GsMTx4 (mechanosensitive ion channel inhibitor, Tocris, 4912/100U) was solubilized in differentiation medium and added to infected

organoids at a final concentration of 20 µM. For experiments in which any compounds solubilized in DMSO were included, the final DMSO concentrations in wells were standardized across all conditions at 0.5% (v/v).

Fractionation of infected organoid cultures

Fractionations of infected organoid suspensions by differential sedimentation in were performed after 8 hours of infection. All samples were kept at 4°C during fractionation. Samples of entire organoid suspension (*Whole Well* samples) were collected in advance of any sedimentation steps. Next, organoids were pelleted by gravity (1 × *g*) for 10 – 15 min. The samples were inspected on a confocal microscope to confirm pelleting of all organoids. The pellets containing intact organoids were washed three times in DMEM and finally resuspended in DMEM for future analysis (*Organoids* samples). The supernatants containing extruded cells in original medium (*Cells + Media* samples) were further spun at 600 × *g* for 3 min to generate *Cells* and *Media* samples. The cell pellets were similarly washed three times in DMEM and resuspended in DMEM for future analysis (*Cells* samples). The supernatants from the 600 × *g* spin were collected (*Media* samples). In experiments with a spike-in of exogenous virus to ensure wash steps were sufficient to remove free virus contamination from cell fractions, 10^6 PFU of EV-A71 virus stock was added to the *Cells + Media* samples and wash steps proceeded as described above. All fractions were subjected to three cycles of freezing and thawing to release intracellular virus in cell- or organoid-containing fractions prior to determination of virus titers by plaque assay.

Secondary infections of organoids and RD cells with cells extruded from infected organoids

Extruded cells from infected organoids were collected as in fractionation experiments above. Following gravity pelleting to remove organoids, extruded *Cells* were flowed through a 70 µm nylon mesh cell strainer. In cases where small organoids were observed flowing through 70 µm strainer, these were removed by an additional 10 × *g* centrifugation for 3 min. During 3rd (final) wash of extruded cells, cold differentiation media was used to wash cells. The supernatant of this wash was retained and used as inoculum on parallel infections to monitor virus levels that may be a result of incomplete removal of cell-free virus. The pellet containing extruded cells was resuspended in cold differentiation media and immediately used as inoculum on new cells or organoids. RD cells secondarily infected were seeded into

24-well plates 1-2 days prior to infection, washed once with Dulbecco's Phosphate Buffered Saline with Ca^{+2} and Mg^{+2} (DPBS++) immediately prior to infection, inoculated for 1 h at 37° C with 150 µL wash supernatant or extruded cells, and washed again with DPBS++ prior to addition of 1 mL per well of RD cell media. Cell media was collected and frozen at -20° C immediately following infection (1 h) or after 16 h infection. Secondary infections of organoids were performed using the methods described above for *EV-A71 infections of organoids*; however, since the immediate use of extruded cells as inoculum made it impossible to quantify viral titer of inoculums prior to their use in secondary infections, secondarily infected cells were not counted for determination of MOI prior to infection.

Statistics and reproducibility

Statistical data analysis was performed in GraphPad Prism 9. Unless otherwise indicated, all experiments were performed three independent times using multiple distinct organoid donor lines to account for donor-specific differences. In microscopy graphs, circles represent measurements of individual organoids (technical replicates) while triangles represent measurements obtained by accumulating data from all organoids from the same experiment (biological replicates). Color of symbols classify independent experiments. This "SuperPlot" graph format used here has been described in detail by Lord *et al* [65]. In all graphs, data are presented as mean ± SD. Information about specific statistical tests in each analysis can be found in the figure legends.

References

1. Taylor, M. P., Burgon, T. B., Kirkegaard, K. & Jackson, W. T. Role of Microtubules in Extracellular Release of Poliovirus. *J. Virol.* **83,** 6599–6609 (2009).

2. Bird, S. W., Maynard, N. D., Covert, M. W. & Kirkegaard, K. Nonlytic viral spread enhanced by autophagy components. *Proc Natl Acad Sci U S A* **111,** 13081–13086 (2014).

3. Hsu, N.-Y., Ilnytska, O., Belov, G., Santiana, M., Chen, Y.-H., Takvorian, P. M., Pau, C., van der Schaar, H., Kaushik-Basu, N., Balla, T., Cameron, C. E., Ehrenfeld, E., van Kuppeveld, F. J. M. & Altan-Bonnet, N. Viral Reorganization of the Secretory Pathway Generates Distinct Organelles for RNA Replication. *Cell* **141,** 799–811 (2010).

4. Feng, Z., Hensley, L., McKnight, K. L., Hu, F., Madden, V., Ping, L., Jeong, S.-H., Walker, C., Lanford, R. E. & Lemon, S. M. A pathogenic picornavirus acquires an envelope by hijacking cellular membranes. *Nature* **496,** 367–371 (2013).

5. Santiana, M., Ghosh, S., Ho, B. A., Rajasekaran, V., Du, W.-L., Mutsafi, Y., De Jésus-Diaz, D. A., Sosnovtsev, S. V., Levenson, E. A., Parra, G. I., Takvorian, P. M., Cali, A., Bleck, C., Vlasova, A. N., Saif, L. J., Patton, J. T., Lopalco, P., Corcelli, A., Green, K. Y. & Altan-Bonnet, N. Vesicle-Cloaked Virus Clusters Are Optimal Units for Inter-organismal Viral Transmission. *Cell Host Microbe* **24,** 208-220.e8 (2018).

6. Chen, Y.-H., Du, W., Hagemeijer, M. C., Takvorian, P. M., Pau, C., Cali, A., Brantner, C. A., Stempinski, E. S., Connelly, P. S., Ma, H.-C., Jiang, P., Wimmer, E., Altan-Bonnet, G. & Altan-Bonnet, N. Phosphatidylserine Vesicles Enable Efficient En Bloc Transmission of Enteroviruses. *Cell* **160,** 619–630 (2015).

7. Lanik, W., Mara, M., Mihi, B., Coyne, C. & Good, M. Stem Cell-Derived Models of Viral Infections in the Gastrointestinal Tract. *Viruses* **10,** 124 (2018).

8. García-Rodríguez, I., Sridhar, A., Pajkrt, D. & Wolthers, K. C. Put some guts into it: Intestinal organoid models to study viral infection. *Viruses* **12,** 1288 (2020).

9. Sato, T., Stange, D. E., Ferrante, M., Vries, R. G. J., Van Es, J. H., Van Den Brink, S., Van Houdt, W. J., Pronk, A., Van Gorp, J., Siersema, P. D. & Clevers, H. Long-term Expansion of Epithelial Organoids From Human Colon, Adenoma, Adenocarcinoma, and Barrett's Epithelium. *Gastroenterology* **141,** 1762–1772 (2011).

10. Drummond, C. G., Bolock, A. M., Ma, C., Luke, C. J., Good, M. & Coyne, C. B. Enteroviruses infect human enteroids and induce antiviral signaling in a cell lineage-specific manner. *Proc Natl Acad Sci U S A* **114,** 1672–1677 (2017).

11. Good, C., Wells, A. I. & Coyne, C. B. Type III interferon signaling restricts enterovirus 71 infection of goblet cells. *Sci. Adv.* **5,** eaau4255 (2019).

12. Zhao, X., Li, C., Liu, X., Chiu, M. C., Wang, D., Wei, Y., Chu, H., Cai, J.-P., Hau-Yee Chan, I., Kak-Yuen Wong, K., Fuk-Woo Chan, J., Kai-Wang To, K., Yuen, K. Y. & Zhou, J. Human Intestinal Organoids Recapitulate Enteric Infections of Enterovirus and Coronavirus. *Stem Cell Reports* **16,** 1–12 (2021).

13. Co, J. Y., Margalef-Català, M., Monack, D. M. & Amieva, M. R. Controlling the polarity of human gastrointestinal organoids to investigate epithelial biology and infectious diseases. *Nat. Protoc.* **16,** 5171–5192 (2021).

14. Co, J. Y., Margalef-Català, M., Li, X., Mah, A. T., Kuo, C. J., Monack, D. M. & Amieva, M. R. Controlling Epithelial Polarity: A Human Enteroid Model for Host-Pathogen Interactions. *Cell Rep.* **26,** 2509–2520 (2019).

15. Witsø, E., Palacios, G., Rønningen, K. S., Cinek, O., Janowitz, D., Rewers, M., Grinde, B. & Lipkin, W. I. Asymptomatic circulation of HEV71 in Norway. *Virus Res.* **123,** 19–29 (2007).

16. Javadi, M., Nejati, A., Yousefi, M., Mahmoodi, M., Shoja, Z. & Shahmahmoodi, S. First seroepidemiological investigation of human enterovirus 71 in Iran. *Iran. J. Microbiol.* **13,** 502–508 (2021).

17. Wu, Q., Fu, X., Jiang, L., Yang, R., Cun, J., Zhou, X., Zhou, Y., Xiang, Y., Gu, W., Fan, J., Li, H. & Xu, W. Prevalence of enteroviruses in healthy populations and excretion of pathogens in patients with hand, foot, and mouth disease in a highly endemic area of southwest China. *PLoS One* **12,** e0181234 (2017).

18. Heybrock, S., Kanerva, K., Meng, Y., Ing, C., Liang, A., Xiong, Z.-J., Weng, X., Kim, Y. A., Collins, R., Trimble, W., Pomès, R., Privé, G. G., Annaert, W., Schwake, M., Heeren, J., Lüllmann-Rauch, R., Grinstein, S., Ikonen, E., Saftig, P. & Neculai, D. Lysosomal integral membrane protein-2 (LIMP-2/ SCARB2) is involved in lysosomal cholesterol export. *Nat. Commun.* **10,** 3521 (2019).

19. Yamayoshi, S., Yamashita, Y., Li, J., Hanagata, N., Minowa, T., Takemura, T. & Koike, S. Scavenger receptor B2 is a cellular receptor for enterovirus 71. *Nat. Med.* **15,** 798–801 (2009).

20. Cheng, H. & Leblond, C. P. Origin, differentiation and renewal of the four main epithelial cell types in the mouse small intestine V. Unitarian theory of the origin of the four epithelial cell types. *Am. J. Anat.* **141,** 537–561 (1974).

21. Leblond, C. P. & Walker, B. E. Renewal of cell populations. *Physiol. Rev.* **36,** 255–76 (1956).

22. Darwich, A. S., Aslam, U., Ashcroft, D. M. & Rostami-Hodjegan, A. Meta-analysis of the turnover of intestinal epithelia in preclinical animal species and humans. *Drug Metab. Dispos.* **42,** 2016–22 (2014).

23. Wang, Y.-F., Chou, C.-T., Lei, H.-Y., Liu, C.-C., Wang, S.-M., Yan, J.-J., Su, I.-J., Wang, J.-R., Yeh, T.-M., Chen, S.-H. & Yu, C.-K. A Mouse-Adapted Enterovirus 71 Strain Causes Neurological Disease in Mice after Oral Infection. *J. Virol.* **78,** 7916–7924 (2004).

24. Chen, S.-C., Chang, L.-Y., Wang, Y.-W., Chen, Y.-C., Weng, K.-F., Shih, S.-R. & Shih, H.-M. Sumoylation-promoted Enterovirus 71 3C Degradation Correlates with a Reduction in Viral Replication and Cell Apoptosis. *J. Biol. Chem.* **286,** 31373–31384 (2011).

25. Dwivedi, V. K., Pardo-Pastor, C., Droste, R., Kong, J. N., Tucker, N., Denning, D. P., Rosenblatt, J. & Horvitz, H. R. Replication stress promotes cell elimination by extrusion. *Nature* **593,** 591–596 (2021).

26. Tanimura, N. & Fujita, Y. Epithelial defense against cancer (EDAC). *Semin. Cancer Biol.* **63,** 44–48 (2020).

27. Brás-Pereira, C. & Moreno, E. Mechanical cell competition. *Curr. Opin. Cell Biol.* **51,** 15–21 (2018).

28. Rosenblatt, J., Raff, M. C. & Cramer, L. P. An epithelial cell destined for apoptosis signals its neighbors to extrude it by an actin- and myosin-dependent mechanism. *Curr. Biol.* **11,** 1847–1857 (2001).

29. Madara, J. L. Maintenance of the macromolecular barrier at cell extrusion sites in intestinal epithelium: Physiological rearrangement of tight junctions. *J. Membr. Biol.* **116,** 177–184 (1990).

30. Guan, Y., Watson, A. J. M., Marchiando, A. M., Bradford, E., Shen, L., Turner, J. R. & Montrose, M. H. Redistribution of the tight junction protein ZO-1 during physiological shedding of mouse intestinal epithelial cells. *Am. J. Physiol. Physiol.* **300,** C1404–C1414 (2011).

31. Andrade, D. & Rosenblatt, J. Apoptotic regulation of epithelial cellular extrusion. *Apoptosis* **16,** 491–501 (2011).

32. Chang, Y.-L., Ho, B.-C., Sher, S., Yu, S.-L. & Yang, P.-C. miR-146a and miR-370 coordinate enterovirus 71-induced cell apoptosis through targeting SOS1 and GADD45β. *Cell. Microbiol.* **17,** 802–818 (2015).

33. Chi, C., Sun, Q., Wang, S., Zhang, Z., Li, X., Cardona, C. J., Jin, Y. & Xing, Z. Robust antiviral responses to enterovirus 71 infection in human intestinal epithelial cells. *Virus Res.* **176,** 53–60 (2013).

34. Li, M.-L., Lin, J.-Y., Chen, B.-S., Weng, K.-F., Shih, S.-R., Calderon, J. D., Tolbert, B. S. & Brewer, G. EV71 3C protease induces apoptosis by cleavage of hnRNP A1 to promote apaf-1 translation. *PLoS One* **14,** e0221048 (2019).

35. Liang, C.-C., Sun, M.-J., Lei, H.-Y., Chen, S.-H., Yu, C.-K., Liu, C.-C., Wang, J.-R. & Yeh, T.-M. Human endothelial cell activation and apoptosis induced by enterovirus 71 infection. *J. Med. Virol.* **74,** 597–603 (2004).

36. Eisenhoffer, G. T., Loftus, P. D., Yoshigi, M., Otsuna, H., Chien, C.-B., Morcos, P. A. & Rosenblatt, J. Crowding induces live cell extrusion to maintain homeostatic cell numbers in epithelia. *Nature* **484,** 546–549 (2012).

37. Gudipaty, S. A. & Rosenblatt, J. Epithelial cell extrusion: Pathways and pathologies. *Semin. Cell Dev. Biol.* **67,** 132–140 (2017).

38. Knodler, L. A., Vallance, B. A., Celli, J., Winfree, S., Hansen, B., Montero, M. & Steele-Mortimer, O. Dissemination of invasive Salmonella via bacterial-induced extrusion of mucosal epithelia. *Proc. Natl. Acad. Sci. U. S. A.* **107,** 17733–8 (2010).

39. Suchyna, T. M., Johnson, J. H., Hamer, K., Leykam, J. F., Gage, D. A., Clemo, H. F., Baumgarten, C. M. & Sachs, F. Identification of a Peptide Toxin from Grammostola spatulata Spider Venom That Blocks Cation-Selective Stretch-Activated Channels. *J. Gen. Physiol.* **115,** 583–598 (2000).

40. Bae, C., Sachs, F. & Gottlieb, P. A. The Mechanosensitive Ion Channel Piezo1 Is Inhibited by the Peptide GsMTx4. *Biochemistry* **50,** 6295–6300 (2011).

41. Gagliardi, P. A., Somale, D., Puliafito, A., Chiaverina, G., di Blasio, L., Oneto, M., Bianchini, P.,

Bussolino, F. & Primo, L. MRCKα is activated by caspase cleavage to assemble an apical actin ring for epithelial cell extrusion. *J. Cell Biol.* **217,** 231–249 (2018).

42. Várkuti, B. H., Képiró, M., Horváth, I. Á., Végner, L., Ráti, S., Zsigmond, Á., Hegyi, G., Lenkei, Z., Varga, M. & Málnási-Csizmadia, A. A highly soluble, non-phototoxic, non-fluorescent blebbistatin derivative. *Sci. Rep.* **6,** 26141 (2016).

43. Kuipers, D., Mehonic, A., Kajita, M., Peter, L. L., Fujita, Y., Duke, T., Charras, G. & Gale, J. E. Epithelial repair is a two-stage process driven first by dying cells and then by their neighbours. *J. Cell Sci.* **127,** 1229–1241 (2014).

44. Bastounis, E. E., Serrano-Alcalde, F., Radhakrishnan, P., Engström, P., Gómez-Benito, M. J., Oswald, M. S., Yeh, Y.-T., Smith, J. G., Welch, M. D., García-Aznar, J. M. & Theriot, J. A. Mechanical competition triggered by innate immune signaling drives the collective extrusion of bacterially infected epithelial cells. *Dev. Cell* **56,** 443-460.e11 (2021).

45. Lin, J.-Y., Weng, K.-F., Chang, C.-K., Gong, Y.-N., Huang, G.-J., Lee, H.-L., Chen, Y.-C., Huang, C.-C., Lu, J.-Y., Huang, P.-N., Chiang, H.-J., Chen, C.-M. & Shih, S.-R. Enterovirus A71 Induces Neurological Diseases and Dynamic Variants in Oral Infection of Human SCARB2-Transgenic Weaned Mice. *J. Virol.* **95,** 897–918 (2021).

46. Miwatashi, W., Ishida, M., Takashino, A., Kobayashi, K., Yamaguchi, M., Shitara, H. & Koike, S. Mouse Scarb2 Modulates EV-A71 Pathogenicity in Neonatal Mice. *J. Virol.* e00561-22 (2022). doi:10.1128/jvi.00561-22

47. Gnanasambandam, R., Ghatak, C., Yasmann, A., Nishizawa, K., Sachs, F., Ladokhin, A. S., Sukharev, S. I. & Suchyna, T. M. GsMTx4: Mechanism of Inhibiting Mechanosensitive Ion Channels. *Biophys. J.* **112,** 31–45 (2017).

48. Gudipaty, S. A., Lindblom, J., Loftus, P. D., Redd, J., Edes, K., Davey, F., Krishnegowda, V. & Rosenblatt, & J. Mechanical stretch triggers rapid epithelial cell division through Piezo1. *Nature*

543, 118–121 (2017).

49. Ge, J., Li, W., Zhao, Q., Li, N., Chen, M., Zhi, P., Li, R., Gao, N., Xiao, B. & Yang, M. Architecture of the mammalian mechanosensitive Piezo1 channel. *Nature* **527,** 64–69 (2015).

50. Schlegel, A. & Kirkegaard, K. in *Hum. Enterovirus Infect.* 135–154 (ASM Press, 2014). doi:10.1128/9781555818326.ch6

51. Armer, H., Moffat, K., Wileman, T., Belsham, G. J., Jackson, T., Duprex, W. P., Ryan, M. & Monaghan, P. Foot-and-Mouth Disease Virus, but Not Bovine Enterovirus, Targets the Host Cell Cytoskeleton via the Nonstructural Protein 3Cpro. *J. Virol.* **82,** 10556–10566 (2008).

52. Badorff, C., Lee, G.-H., Lamphear, B. J., Martone, M. E., Campbell, K. P., Rhoads, R. E. & Knowlton, K. U. Enteroviral protease 2A cleaves dystrophin: Evidence of cytoskeletal disruption in an acquired cardiomyopathy. *Nat. Med.* **5,** 320–326 (1999).

53. Cudmore, S., Reckmann, I. & Way, M. Viral manipulations of the actin cytoskeleton. *Trends Microbiol.* **5,** 142–8 (1997).

54. Ploubidou, A. & Way, M. Viral transport and the cytoskeleton. *Curr. Opin. Cell Biol.* **13,** 97–105 (2001).

55. Cox, C. D., Bae, C., Ziegler, L., Hartley, S., Nikolova-Krstevski, V., Rohde, P. R., Ng, C.-A., Sachs, F., Gottlieb, P. A. & Martinac, B. Removal of the mechanoprotective influence of the cytoskeleton reveals PIEZO1 is gated by bilayer tension. *Nat. Commun.* **7,** 10366 (2016).

56. Yang, J. E., Rossignol, E. D., Chang, D., Zaia, J., Forrester, I., Raja, K., Winbigler, H., Nicastro, D., Jackson, W. T. & Bullitt, E. Complexity and ultrastructure of infectious extracellular vesicles from cells infected by non-enveloped virus. *Sci. Rep.* **10,** 7939 (2020).

57. Erickson, A. K., Jesudhasan, P. R., Mayer, M. J., Narbad, A., Winter, S. E. & Pfeiffer, J. K. Bacteria Facilitate Enteric Virus Co-infection of Mammalian Cells and Promote Genetic

Recombination. *Cell Host Microbe* **23,** 77-88.e5 (2018).

58. Brown, J. J., Short, S. P., Stencel-Baerenwald, J., Urbanek, K., Pruijssers, A. J., Mcallister, N., Ikizler, M., Taylor, G., Aravamudhan, P., Khomandiak, S., Jabri, B., Williams, C. S. & Dermody, T. S. Reovirus-Induced Apoptosis in the Intestine Limits Establishment of Enteric Infection. *J. Virol.* **92,** e02062-17 (2018).

59. Zhu, S., Ding, S., Wang, P., Wei, Z., Pan, W., Palm, N. W., Yang, Y., Yu, H., Li, H.-B., Wang, G., Lei, X., de Zoete, M. R., Zhao, J., Zheng, Y., Chen, H., Zhao, Y., Jurado, K. A., Feng, N., Shan, L., Kluger, Y., Lu, J., Abraham, C., Fikrig, E., Greenberg, H. B. & Flavell, R. A. Nlrp9b inflammasome restricts rotavirus infection in intestinal epithelial cells. *Nature* **546,** 667–670 (2017).

60. Pickles, R. J. & DeVincenzo, J. P. Respiratory syncytial virus (RSV) and its propensity for causing bronchiolitis. *J. Pathol.* **235,** 266–276 (2015).

61. Eckardt-Michel, J., Lorek, M., Baxmann, D., Grunwald, T., Keil, G. M. & Zimmer, G. The Fusion Protein of Respiratory Syncytial Virus Triggers p53-Dependent Apoptosis. *J. Virol.* **82,** 3236–3249 (2008).

62. Hippee, C. E., Singh, B. K., Thurman, A. L., Cooney, A. L., Pezzulo, A. A., Cattaneo, R. & Sinn, P. L. Measles virus exits human airway epithelia within dislodged metabolically active infectious centers. *PLOS Pathog.* **17,** e1009458 (2021).

63. Miyoshi, H. & Stappenbeck, T. S. In vitro expansion and genetic modification of gastrointestinal stem cells in spheroid culture. *Nat. Protoc.* **8,** 2471–2482 (2013).

64. Huang, S.-W., Wang, Y.-F., Yu, C.-K., Su, I.-J. & Wang, J.-R. Mutations in VP2 and VP1 capsid proteins increase infectivity and mouse lethality of enterovirus 71 by virus binding and RNA accumulation enhancement. *Virology* **422,** 132–143 (2012).

65. Lord, S. J., Velle, K. B., Mullins, R. D. & Fritz-Laylin, L. K. SuperPlots: Communicating

reproducibility and variability in cell biology. *J. Cell Biol.* **219,** (2020).

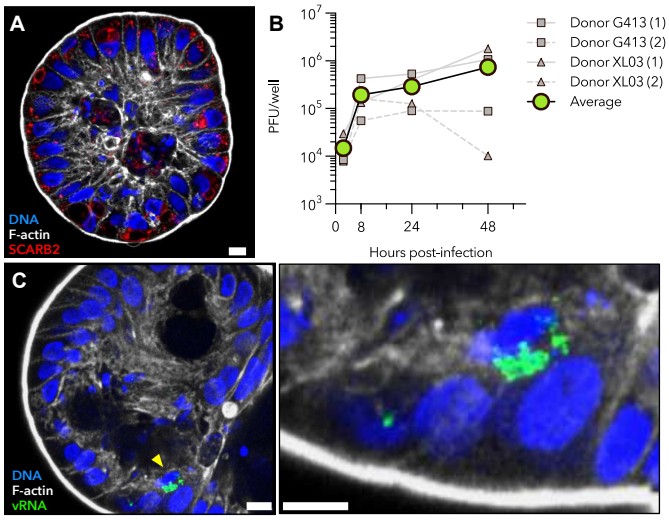

Fig 1: Apical-out colon organoids are permissive to EV-A71 infection. (A) Apical-out, differentiated colon epithelial organoids express the Enterovirus 71 (EV-A71) receptor SCARB2 (red), localizing to intracellular membranes. The integrity of the apical actin (white) microvillus brush border is visible. (B) Colon organoids were infected with EV-A71. Viral titers were monitored over time by plaque assay. Data from four independent experiments using two different colonoid donors are shown. (C) EV-A71-infected cells were observed by immunofluorescence assay following staining for double-stranded viral RNA (vRNA) after 48 hours of infection. Right panel: increased magnification of infected cell denoted by yellow arrowhead in left panel. All scale bars equal 10 μm.

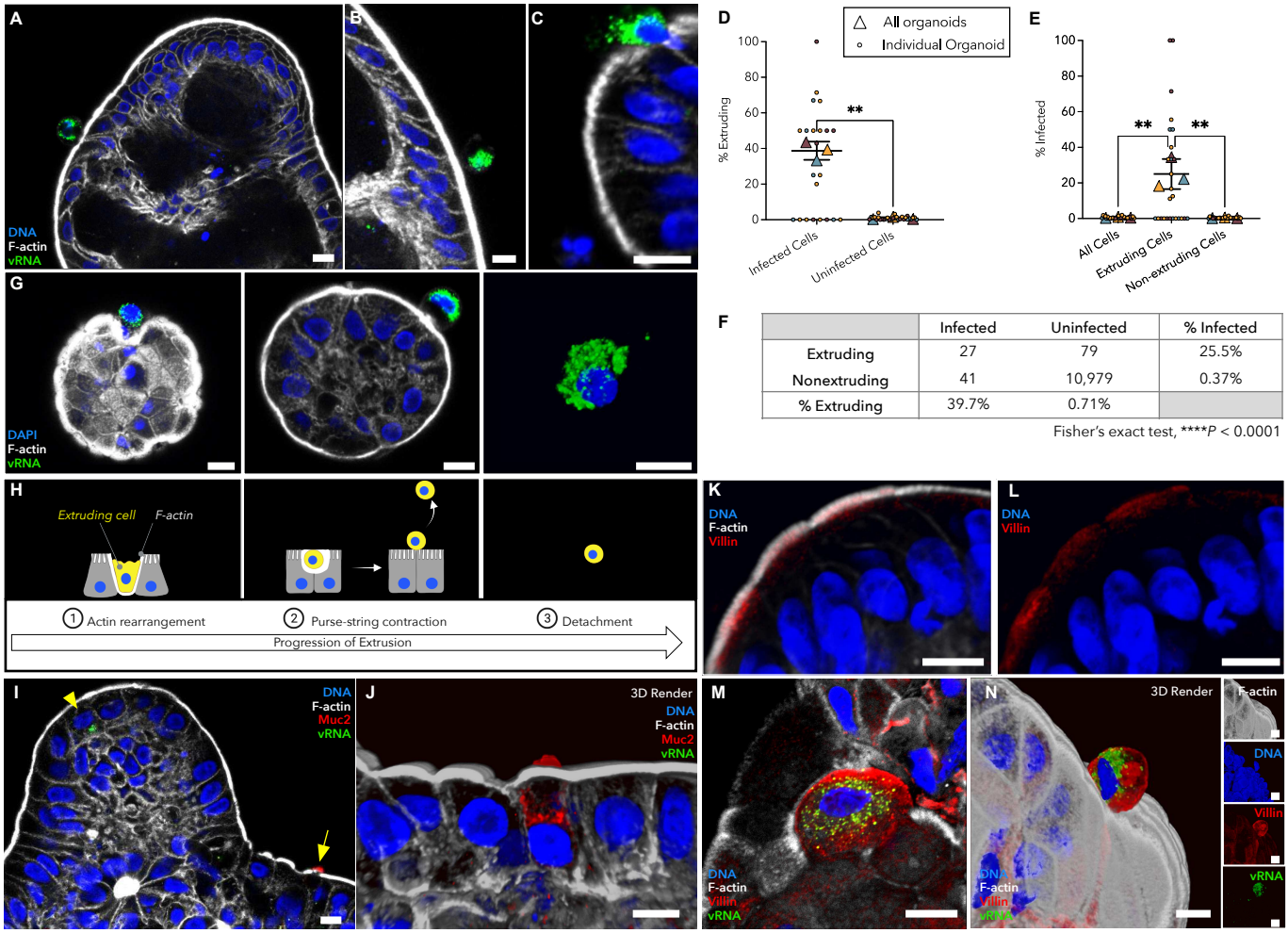

F

	Infected	Uninfected	% Infected
Extruding	27	79	25.5%
Nonextruding	41	10,979	0.37%
% Extruding	39.7%	0.71%	

Fisher's exact test, ****$P < 0.0001$

Fig 2: EV-A71-infected cells are specifically extruded from colonoids. (A-C) Infected colonoids were fixed at 48 hours post-infection and stained for double-stranded viral RNA. (D) Infected cells were extruded from colonoids with higher frequency than uninfected cells. The percentages of infected or uninfected cells extruding from an individual organoid are shown as small circles. The proportion of cells extruding across all organoids in each experiment are shown as triangles of the same color as the individual colonoids. At least ten organoids quantified per experiment. **$p < 0.01$; Paired t-test, $N = 3$. (E) Percentages of infected extruding and non-extruding cells were measured similarly. Of the cells that were extruding, a higher percentage was infected. **$p < 0.01$; Repeated measures one-way ANOVA with Tukey's multiple comparisons test, $N = 3$. (F) 2x2 contingency table displays the number of cells in groups represented in D-E. Cell numbers are summed from three experiments. (G) Representative extruding infected cells are shown. (H) Stages of canonical cell extrusion in uninfected epithelia are depicted. (I) EV-A71-infected colonoids were stained for Muc2 expression, a marker for goblet cells. Arrowhead indicates infected cell. Arrow indicates goblet cell shown in J. (J) Muc2-expressing goblet cell. (K, L). Villin expression identifies colonocytes. Villin localizes apically, overlapping with the actin-rich microvillus brush border. (M, N) EV-A71-infected colonoids were stained for Villin expression. Distinct individual cells are shown in M and N. All scale bars equal 10 μm.

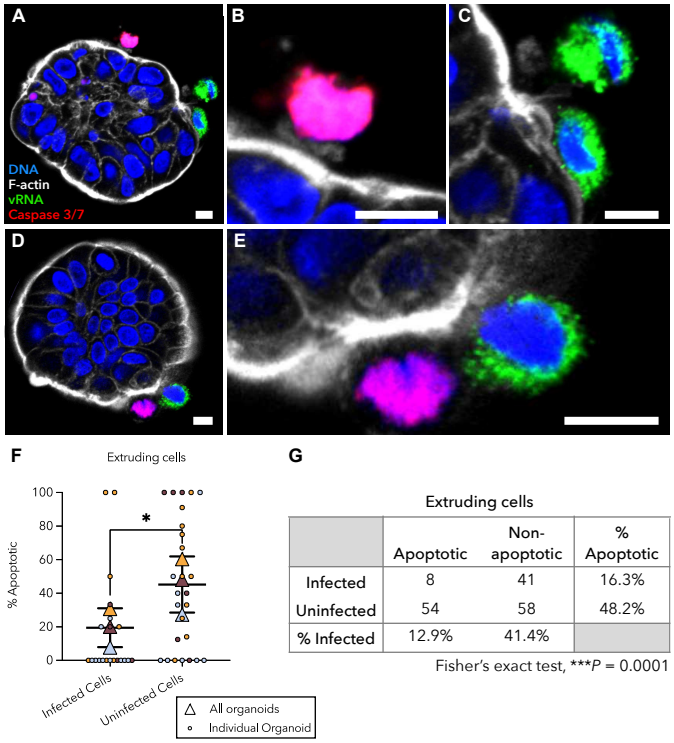

Fig 3: EV-A71-infected cell extrusion is not driven by apoptosis. Infected colonoids were visualized by immunofluorescence confocal microscopy after 48 hours of infection. Caspase 3 and 7 activity was visualized using a fluorogenic substrate. (A and D) Individual infected organoids with extruding cells. (B) Increased magnification of single uninfected, apoptotic extruding cell in A. (C) Increased magnification of two infected, non-apoptotic extruding cells in A. (E) Magnification of two extruding cells in (D). (F) Proportions of infected extruding and uninfected extruding cells that were apoptotic were quantified, with overall values for each experiment shown as triangles. Each color represents an independent experiment, with measurements for each individual organoid shown as small circles. *$p < 0.05$; Paired t-test, $N = 3$. (G) 2x2 contingency table displays the number of cells in each group. Cell numbers are summed from all three independent experiments depicted in F. All scale bars equal 10 μm.

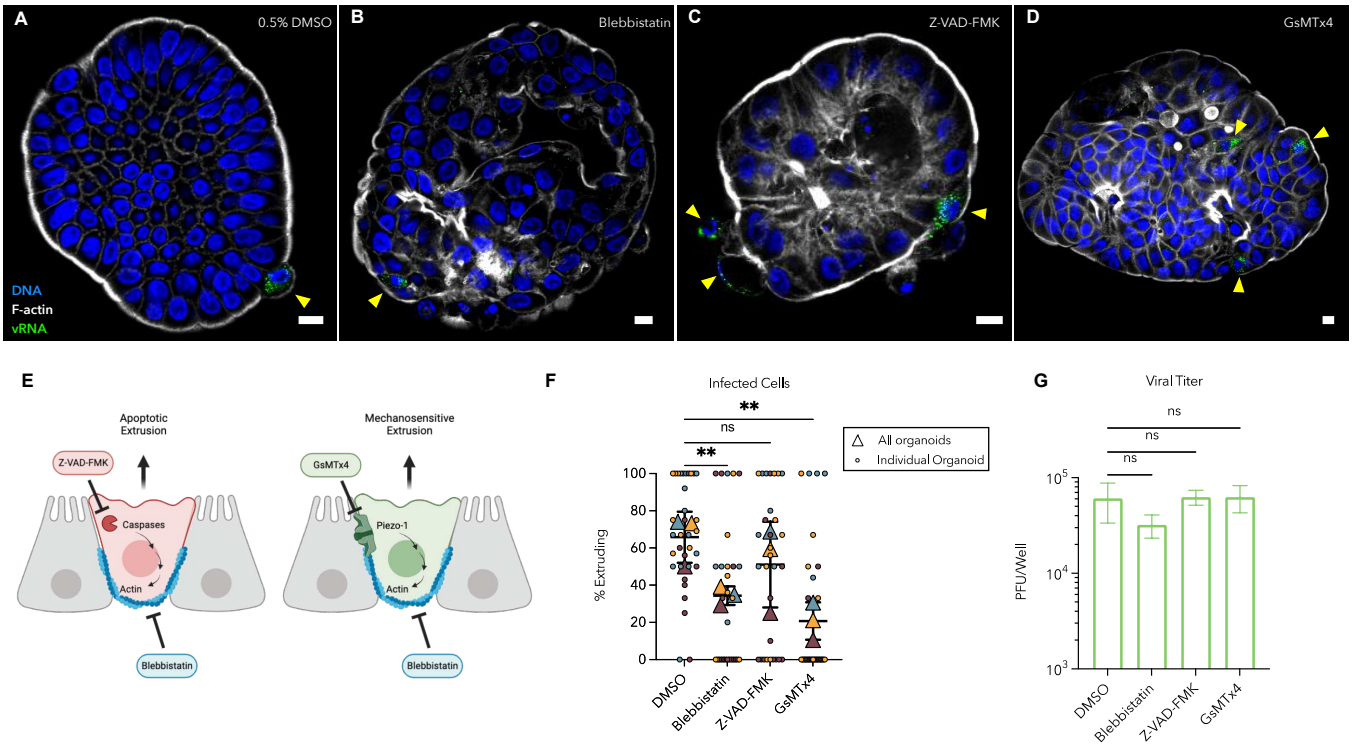

Fig 4: Mechanosensitive signaling facilitates EV-A71 infected cell extrusion. EV-A71-infected organoids were exposed to compounds capable of inhibiting cellular factors implicated in different mechanisms of extrusion, as depicted in E. Infected organoids were exposed to (A) 0.5% DMSO vehicle control, (B) 50 μM para-nitro-blebbistatin, (C) 100 μM Z-VAD-FMK, or (D) 20 μM GsMTx4. Infected cells in organoids were visually inspected by confocal microscopy. Yellow arrowheads indicate infected cells in representative organoids. Scale bars equal 10 μm. (E) Blebbistatin inhibits both apoptotic and mechanosensitive extrusions, Z-VAD-FMK inhibits only apoptotic extrusion, and GsMTx4 inhibits only mechanosensitive extrusion. (F) The percentage of infected cells undergoing extrusion after seven hours of infection was enumerated. Each color shows an independent experiment. Overall proportion of infected cells extruding per experiment shown as triangles, with measurements for each organoid shown as small circles. $^{**}p < 0.01$; Repeated measures one-way ANOVA with Dunnett's multiple comparisons test, $N = 3$. (G) Viral titers quantified at seven hours post-infection from infected suspension organoid cultures show no significant effects of drug treatments on virus yield. Repeated measures one-way ANOVA with Dunnett's multiple comparisons test, $N = 3$.

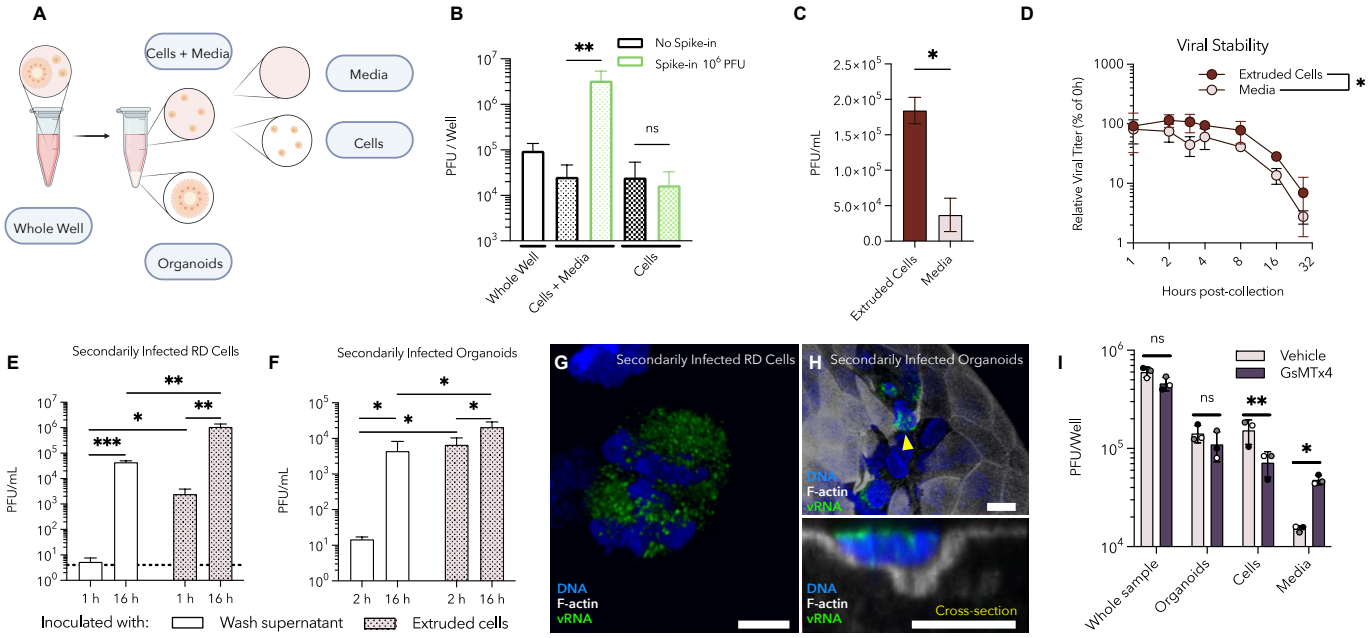

Fig 5: Extruded cells are infectious to cell monolayers and to organoids. (A) EV-A71 infected colonoid cultures were harvested at 8 h post-infection, and components were isolated by differential sedimentation. (B) To assess effectiveness of washing extruded cells, 10^6 PFU exogenous free virus was spiked-in to Cells + Media samples. Fractions were subjected to freeze-thaw and titer determined by plaque assay. $^{**}p < 0.01$; repeated measures one-way ANOVA with the Holm-Sidak multiple comparisons test. (C) Distribution of virus in *Cells* and in *Media*. $^{*}p < 0.05$; ratio paired t-test. (D) Stability of virus from *Cells* and *Media* fractions. Collected fractions were incubated at 37° C for the times indicated, subjected to repetitive freeze/thaw, and amounts of infectious virus measured by plaque assay. Amounts of virus are normalized to initial values from (C) before incubation. $^{*}p < 0.05$; two-way ANOVA with Geisser's-Greenhouse correction. (E) Intact extruded *Cells* fractions and free virus from the final wash of *Cells* were used to infect RD cell monolayers. Viral titers in the infected RD cells were measured 1 h and 16 h after initiating secondary infection. $^{*}p < 0.05$; ratio paired t-test used for paired infection comparisons; unpaired t-test used for unpaired infection comparisons (wash – cells). Dashed line indicates limit of detection. (F) *Cells* fractions and free virus from the final wash of *Cells* were used to infect new colonoids. After 2 h and 16 h and the amount of virus in *Whole Well* fractions was determined by plaque assay. (G-H) Confocal microscopy of secondarily infected (G) RD cells and (H) organoids inoculated with *Cells* after 16 hours. Scale bars equal 10 μm. (H) Secondarily infected organoid with several infected cells. Bottom: orthogonal cross-section through the secondarily infected, extruding cell indicated by yellow arrowhead. (I) EV-A71-infected colonoid cultures were treated with GsMTx4 or vehicle control and fractions harvested after 8 h. While GsMTx4 treatment reduced the amount of infectious virus in extruded cells, the amount of infectious free virus in the media increased. $^{*}p < 0.05$, $^{**}p < 0.01$; multiple paired t-tests with the Holm-Sidak correction for multiple comparisons. In (B-F, I) one representative experiment is shown with independent infections performed in triplicate.

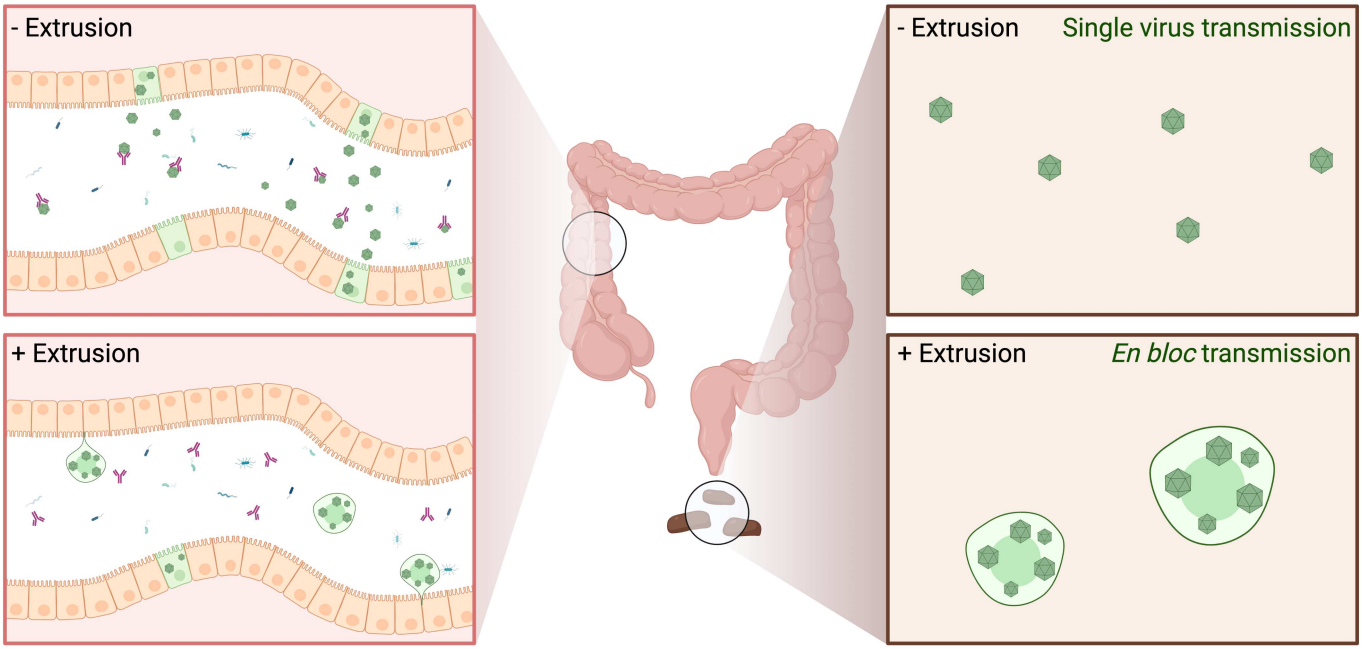

Fig 6: Model for implications of infected cell extrusion on EV-A71 spread. EV-A71-infected cells extruded from the colon into the gastrointestinal lumen may play an integral role in fecal-oral transmission. When cells carrying infectious virus are extruded, progeny virions are expected to transit through the gut and be excreted in stool within live extruded cells. Within cells, virions may be protected from intestinal contents such as mucosal antibodies. Within-cell bundling of virions might additionally facilitate *en bloc* transmission, allowing for viral genomic diversity to be maintained. The potential for host benefits of infected cell extrusion *in vivo* such as quicker viral clearance or improved tolerance to infection remain intriguing open questions for further study.

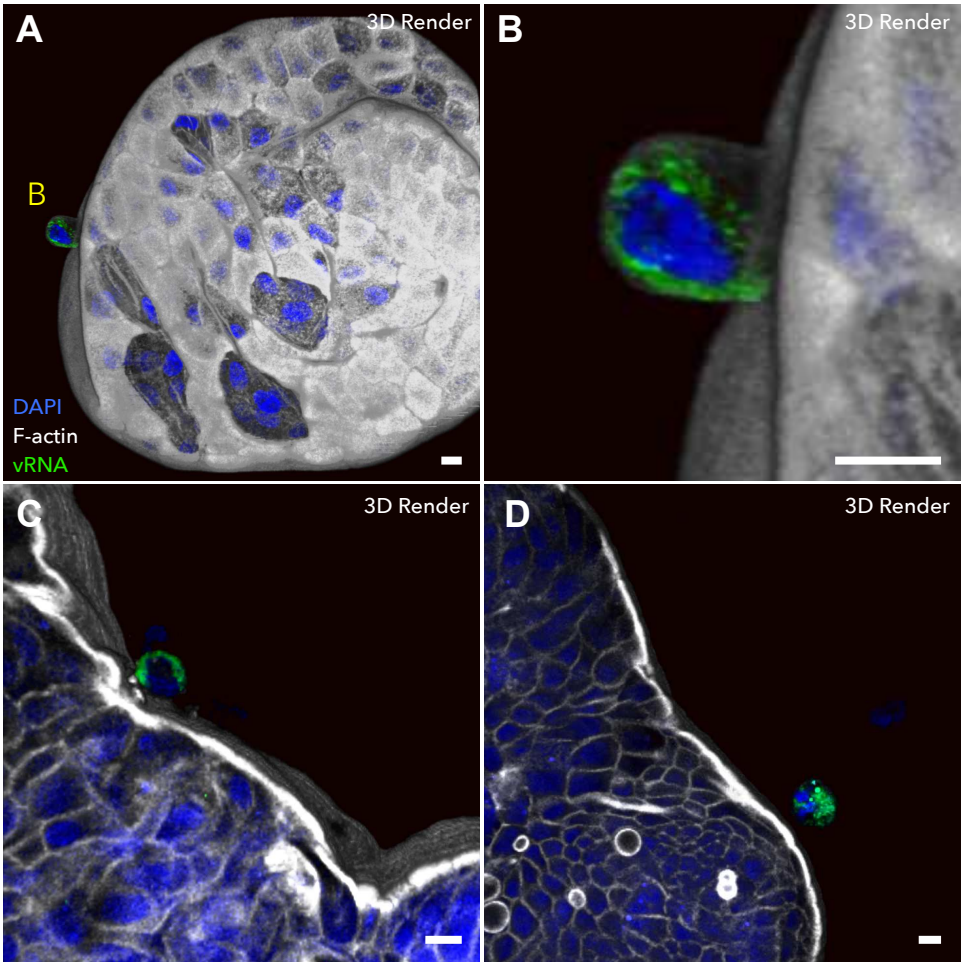

Fig S1: Poliovirus-infected cells extrude from infected ileum and colon organoids. Cells infected with poliovirus Type 1 (Mahoney) were observed extruding from organoids by immunofluorescence. (A) Ileum organoids infected with an MOI = 10 PFU/cell for 22 h. (B) Individual cell highlighted in A (C-D) Colon organoids infected with an MOI = 1 PFU/cell for 42 h. MOI was determined by viral titer on HeLa cells. Scale bars equal 10 μm.

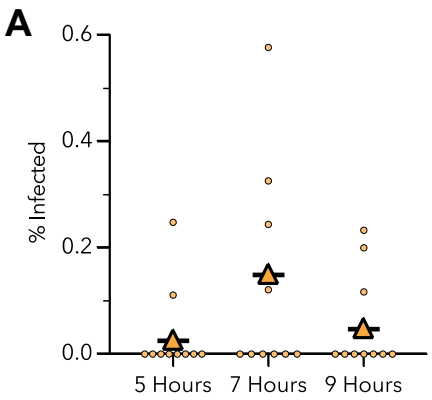

B

	Infected	Uninfected	% Infected
5h	2	8150	0.025%
7h	11	7385	0.149%
9h	3	6439	0.047%

Chi squared test, *P = 0.0106

Fig S2: Infected cells accumulate in organoids after 7 h infection and diminish after 9 h. (A) Infected organoids were fixed at timepoints over the first cycle of infection and the number of infected and uninfected cells were enumerated using fluorescence microscopy. Each dot represents the proportion of infected cells within an individual organoid; triangles represent values averaged across all organoids for each timepoint. One experiment with N = 10 organoids quantified per timepoint. A peak in the proportion of infected cells within organoids emerged at 7 hpi and was reduced after 9 hpi. (B) Total numbers of infected and uninfected cells represented in (A); *P = 0.0106, Chi squared test.

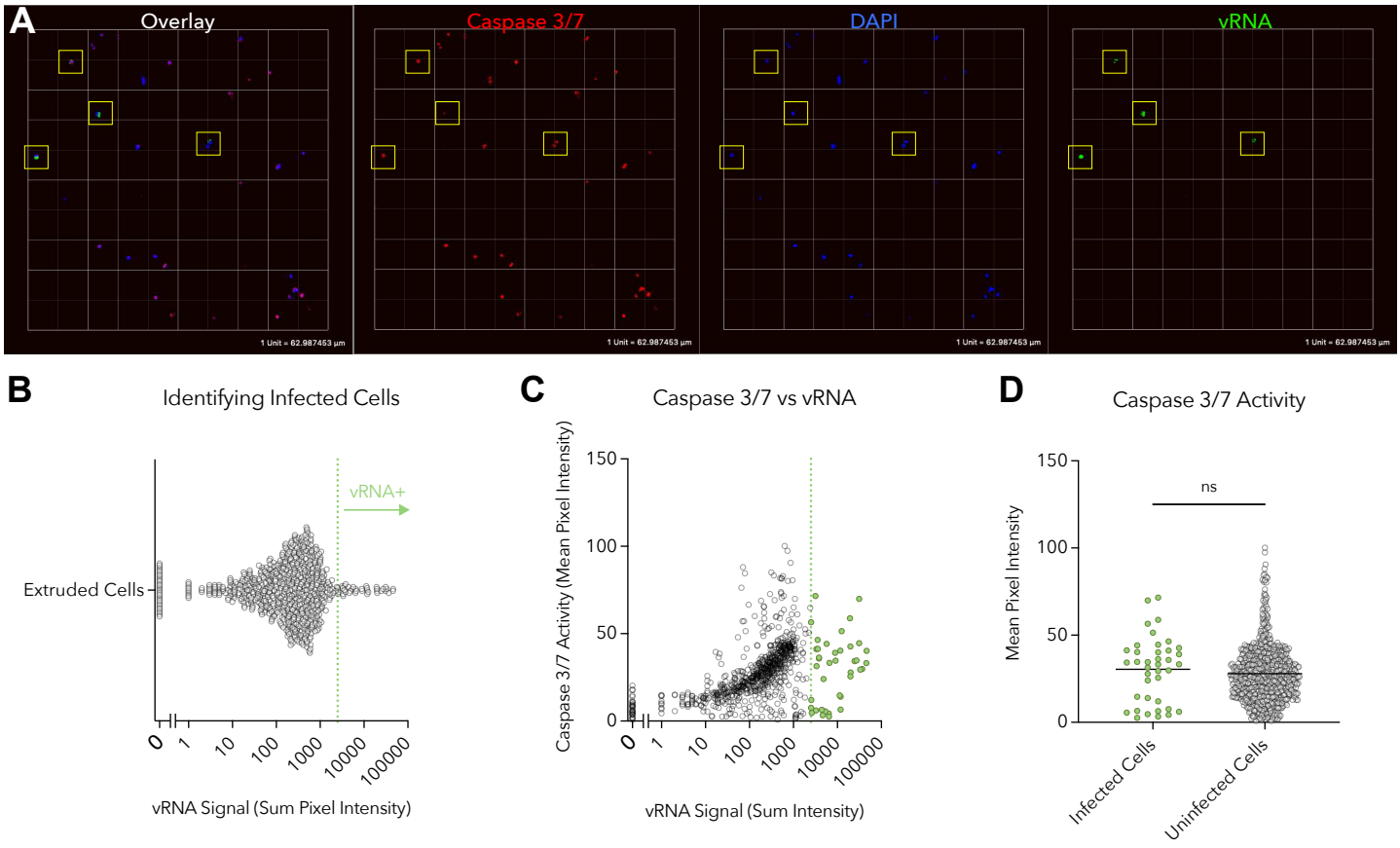

Fig S3: Extruded cells undergo anoikis by 48 hpi. Cells that had fully extruded from infected colonoids in the presence of the fluorogenic caspase 3/7 substrate CellEvent were collected at 48 hpi, fixed, and examined by fluorescence microscopy at 20x magnification. (A) 3D renderings of imaged cells were visualized using Volocity image analysis software. Infected cells are surrounded by yellow boxes. (B) Individual cells were identified from 20 unique fields of view as in *A* using computational measurement tools in Volocity. Data was collected from *N* = 743 individual cells. Cells with a sum pixel intensity greater than 2500 in the vRNA channel were identified as infected; *N* = 39 infected cells, 5.2% of total. (B) Caspase 3/7 activity, as defined by mean pixel intensity, was measured for each cell and plotted as a function of vRNA signal. (C) The caspase 3/7 activity of infected cells was comparable to that of uninfected cells.

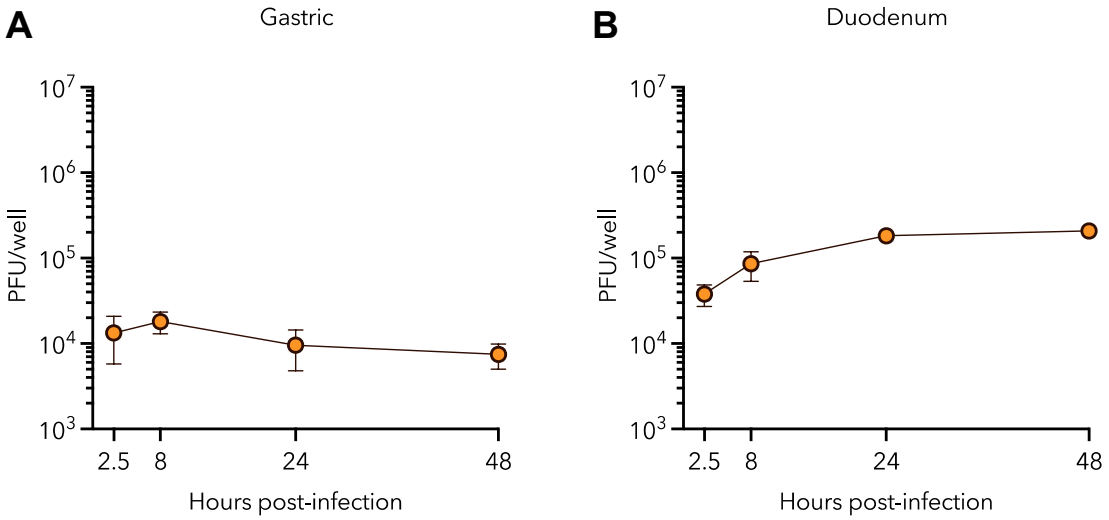

Fig S4: EV71 growth in organoids derived from gastric and duodenal tissue. Apical-out, differentiated epithelial organoids derived from human (A) gastric and (B) duodenal tissue were infected with Enterovirus A-71. Viral titer was monitored over time by plaque assay. Data from one unique donor and experiment per panel are shown in technical triplicate.